# 5 Turbulent Flame Dynamics

The dynamics of a turbulent, swirl-stabilized flame were investigated to elucidate the effects of turbulence and large-scale structures on flame dynamics. Turbulence is known to cause stretch in flames, affecting the flame speed. Large-scale structures strongly affect the stabilization of turbulent flames. The majority of low-NOx combustors in gas turbines are swirl-stabilized, making this study directly applicable to the gas turbine industry. Frequency response functions of the effect of velocity perturbations on OH* chemiluminescence and product gas temperature were measured. The measurements allowed the development of compact, low-order models of the response of reaction rate and the acoustic forcing function to velocity perturbations for turbulent, swirl-stabilized flames.

## 5.1 Objectives

Turbulent, swirl-stabilized flames were studied to analyze the global effects of turbulence and large-scale structures on flame dynamics. Through comparing the dynamics of laminar and turbulent flames, the effect of turbulence can be determined. Measurements of turbulent flame dynamics allow the development of low-order models relevant to the gas turbine and aero-engine industry.

## 5.2 Experimental Procedure

**5.2.1 Measurement Process.** A strict set of procedures was followed each time data was recorded to insure repeatability and validity. At regular intervals – approximately every two tests – the entire flow system was leak-tested to insure laboratory safety and accurate flow measurements. Leak testing was accomplished by pressurizing the flow train and applying soapy water to all connections. First, all electronics (signal conditioning

circuits, diode laser controller, speaker amplifier, etc.) were powered. Then, air was circulated through the rig for no less than 20 minutes to allow the air flow to reach steady-state and rid the flow train of any moisture. Moisture creates errors in the flow meter readings, as well as affecting combustion chemistry. The cooling water flow was started to cool the combustor and optics. The methane flow was then started and the flame lit using a propane torch. Before taking data, the combustor was allowed a minimum of 30 minutes to reach steady state at the desired operating conditions. The combustor, as well as the flow, must reach static temperatures for the reactions, heat transfer, and fluid flow to stabilize. After the flame was lit, the lights were turned off and the photo-multiplier tube (PMT) power supply switched on and the cover removed from the receiving optics. While the combustor was stabilizing, the appropriate speaker levels were mapped to insure measurements represented linear flame dynamics, as described in Section 4.2.1. The diode lasers were aligned, as the density gradients caused by hot product gases have a significant beam-steering effect. Once the combustor had reached steady state and all signals were verified, the Labview program flame_dynamics_step_r1.vi was run to collect data. The program set the speaker to the correct voltage for each desired frequency. After 45 seconds to reach steady state at the excited conditions, the program recorded time-trace data. Steady-state lineshape data was also collected at each frequency for the diode lasers. After collecting data, the program displayed the flow rate and equivalence ratio at each forcing frequency, allowing the researcher to adjust as needed throughout the test. Due to the high heat output of the combustor, changes in ambient temperature made adjustments to the flow and diode laser alignment necessary during the course of a test.

**5.2.2. Frequency Response Data Analysis.** The data acquisition system records time traces of signals. The data was then digitally filtered and scaled. A spectral analysis is performed to obtain frequency response functions. To account for any misalignment of the diode lasers or changes in optical transmission during the test, a reference intensity was calculated at each frequency of excitation using the lineshape data. Aside from this change, the data analysis procedure was identical to the procedure followed to analyze the laminar data (see section 4.2.2).

## 5.3 Experimental Results

Frequency response functions of flame dynamics were measured. OH* chemiluminescence was used as an indicator of chemical heat release rate, or reaction rate. Product gas temperature, measured via TDLAS, provides a measurement of the acoustic forcing function. Frequency response functions were recorded at flow rates of 20 and 25 scfm at equivalence ratios of 0.60 and 0.65 for methane. Block swirlers with vane angles of 45 and 30 degrees were used, resulting in swirl numbers of 0.78 and 0.45.

**5.3.1 OH* Chemiluminescence Frequency Response Functions.** OH* chemiluminescence is an accurate indicator of chemical reaction rate [1]. Measurements of reaction rate dynamics in a turbulent, swirl-stabilized flame are shown in Figure 5.1. Data with coherence above 0.5 is plotted. The bandwidth of the reaction rate dynamics is approximately 320 Hz. At higher frequencies, the coherence drops dramatically, indicating the reaction rate no longer responds. Three dominant resonances are observed: one damped resonance at approximately 120 Hz and two lightly damped modes at around 200 and 280 Hz. For all of the cases studied, the frequency response functions are very similar, as was observed by Khanna [2]. This may be attributed to the basic flow-field and fluid structures remaining the same for all tests. Khanna observed a lightly damped resonance at 275 Hz, which is also seen in this data. This resonance is thought to correspond to flame flapping caused by evanescent waves, as indicated by phase-locked images of the flame presented in Khanna's thesis. Vortex shedding from the sudden expansion into the combustor may also be the cause of the flame flapping.

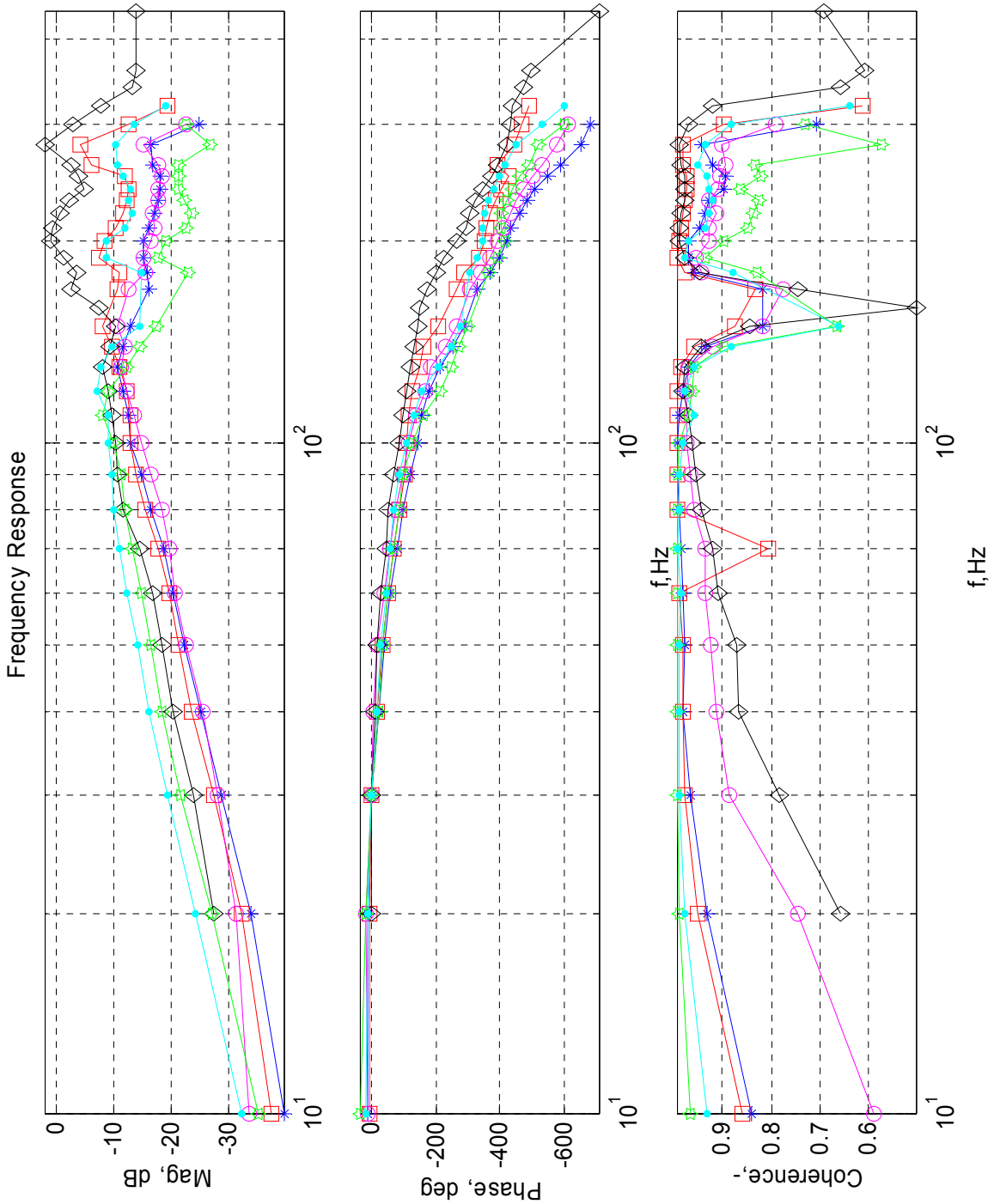
Frequency Response
Mag, dB
0
-10
-20
-30
Phase, deg
0
-200
-400
-600
Coherence,-
0.9
0.8
0.7
0.6
f,Hz
f,Hz
$10^1$
$10^2$

(a)

| Symbol | Qa, scfm | Φ | S |
|---|---|---|---|
| * | 20 | 0.60 | 0.78 |
| □ | 20 | 0.65 | 0.78 |
| ○ | 25 | 0.57 | 0.78 |
| ◊ | 25 | 0.65 | 0.78 |
| ○ | 20 | 0.60 | 0.45 |
| ● | 20 | 0.65 | 0.45 |

(b)

**Figure 5.1. OH* Chemiluminescence Frequency Response Functions.** The frequency responses show similar trends (a) data, (b) legend.

**5.3.1 Temperature Frequency Response Functions.** As discussed in Chapter 1, the temperature oscillations correlate to acoustic forcing function (AFF) dynamics. Measurements of AFF dynamics are shown in Figure 5.2. Data with coherence above 0.5 is plotted. The temperature measurement was taken in the post-flame region. As in the OH* frequency responses, the temperature frequency responses exhibit similar dynamics for the range of conditions studied. There is no appreciable response in temperature at low frequencies, indicating low-frequency perturbations are absorbed by the turbulence in the flame. However, high-frequency oscillations propogate through the combustion region and are amplified. From this observation, it may be postulated that turbulent flame dynamics are governed by reaction rate at low frequencies and by thermal diffusion at high frequencies. The enthalpy caused by unsteady convection in the laminar burner is replaced with thermal diffusion in the turbulent combustor. Turbulence greatly enhances thermal diffusivity, often called turbulent diffusivity. Although the AFF dynamics are very complicated, the dominant features are one resonance at approximately 150 Hz, and one resonance at approximately 850 Hz. Two zeros are evident, as the overall phase drop is close to zero. The phase rises due to zeros cancel the phase drops due to poles.

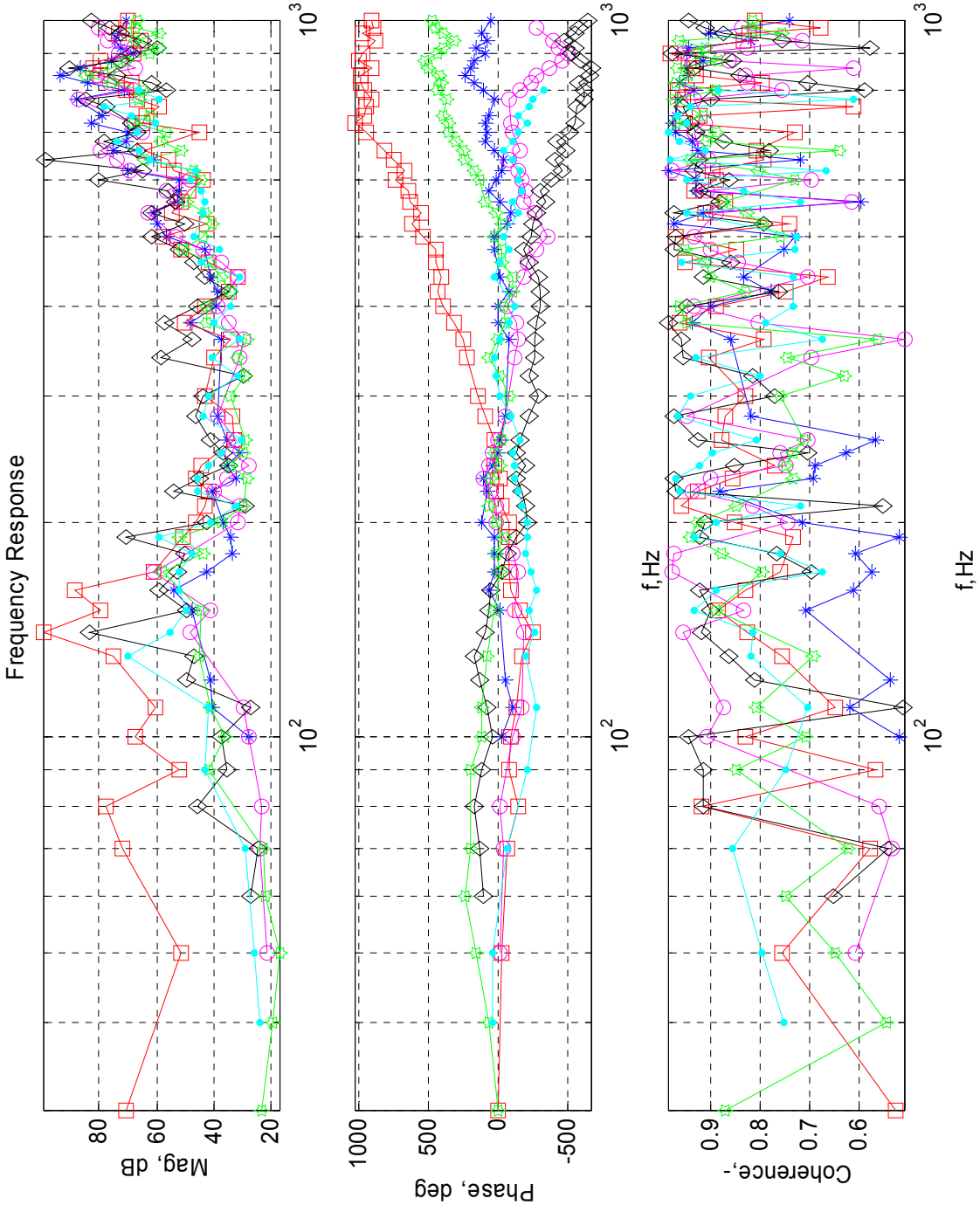
Frequency Response
Mag, dB
80
60
40
20
$10^2$
$10^3$
Phase, deg
1000
500
0
-500
$10^2$
$10^3$
Coherence,-
0.9
0.8
0.7
0.6
$10^2$
$10^3$
f,Hz
f,Hz

(a)

| Symbol | Qa, scfm | Φ | S |
|---|---|---|---|
| * | 20 | 0.60 | 0.78 |
| □ | 20 | 0.65 | 0.78 |
| ○ | 25 | 0.57 | 0.78 |
| ◊ | 25 | 0.65 | 0.78 |
| ○ | 20 | 0.60 | 0.45 |
| ● | 20 | 0.65 | 0.45 |

(b)

**Figure 5.2. Temperature Frequency Response.** Turbulent flames exhibit complicated AFF dynamics. (a) data, (b) legend.

**5.3.3 Chimney Acoustics.** There was concern that the resonances observed in the turbulent flame dynamics were a result of acoustic waves in the chimney section. It is possible that a bulk acoustic mode could oscillate the flow in the chimney section, creating oscillations in heat release rate. However, bulk modes in the chimney would not be measured by the velocity probe, so the increased heat release would look like a resonance. The acoustics of the chimney section were measured with an without the flame by forcing the loudspeaker with random noise and measuring the pressure in the chimney. Figure 5.3 shows the frequency response of the pressure signal to the speaker excitation with no flame. No significant acoustic resonances are observed that would interact with the flame. Figure 5.4 shows the frequency response when the flame is lit at Qa=20 scfm, equivalence ratio = 0.60, and S=0.45. Even at forcing amplitudes much greater than used in the flame dynamics measurements, no acoustic resonances are observed. Thus, the resonances in turbulent flame dynamics are not due to bulk modes in the chimney.

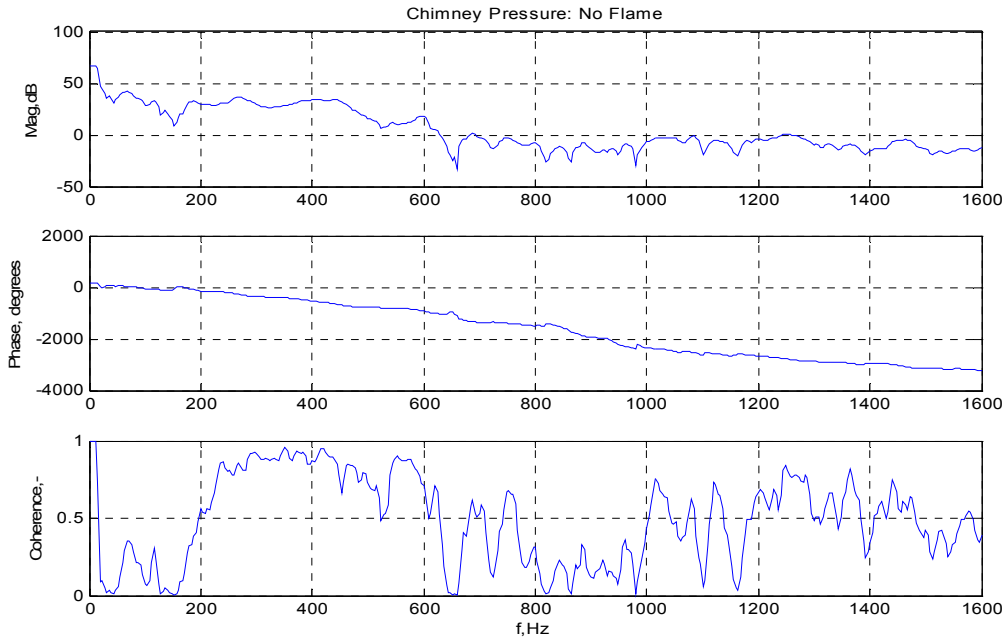


**Figure 5.3 Chimney Pressure: No Flame.** The chimney pressure shows no significant acoustic resonances.

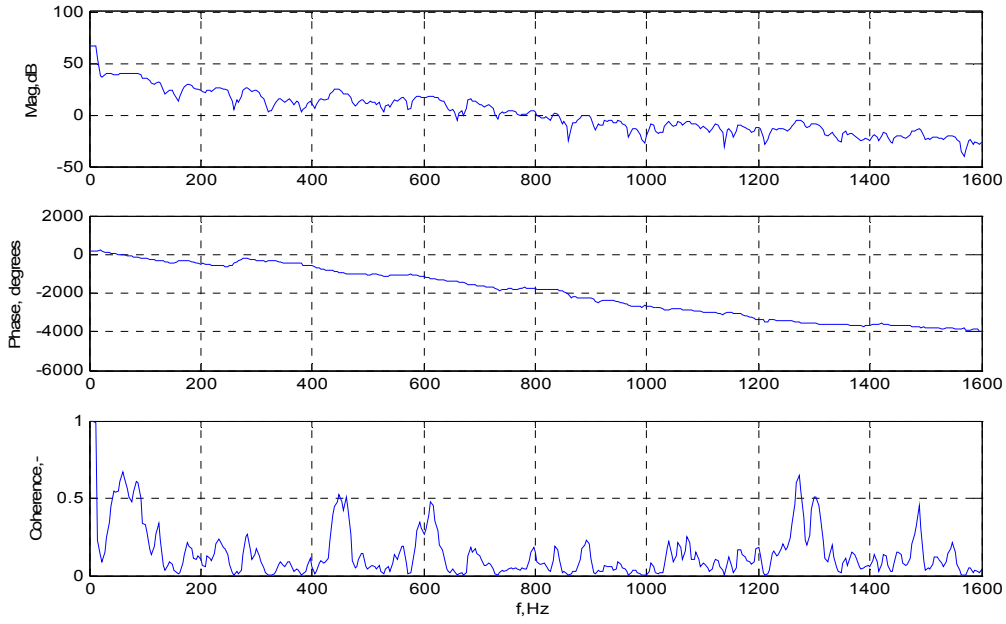


**Figure 5.4 Chimney Pressure: with Flame.** No acoustic resonances are observed at high forcing amplitudes.

**5.3.4 Comparison of Laminar and Turbulent Flame Dynamics.** The reaction rate dynamics for laminar and turbulent flames are compared in Figure 5.5. The dominant resonance, in the 80 to 150 Hz range, coincides closely for the laminar and turbulent dynamics. However, the turbulent flame exhibits two high-frequency resonances not observed in the laminar flame. This results in 360 degrees of additional phase drop than in the laminar FRF. The divergence suggests the two high-frequency resonances in reaction rate are related to turbulence.

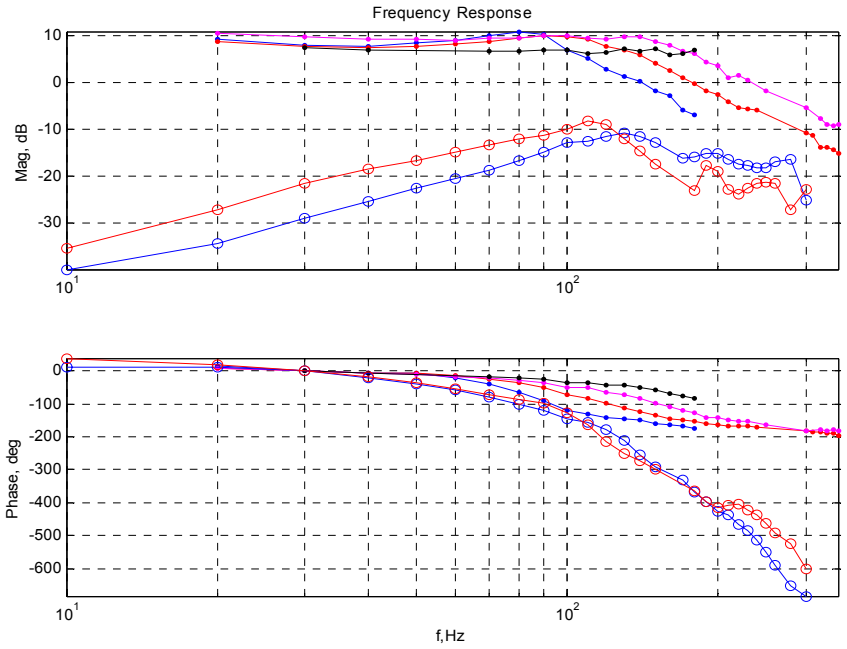


(a) Φ=0.60

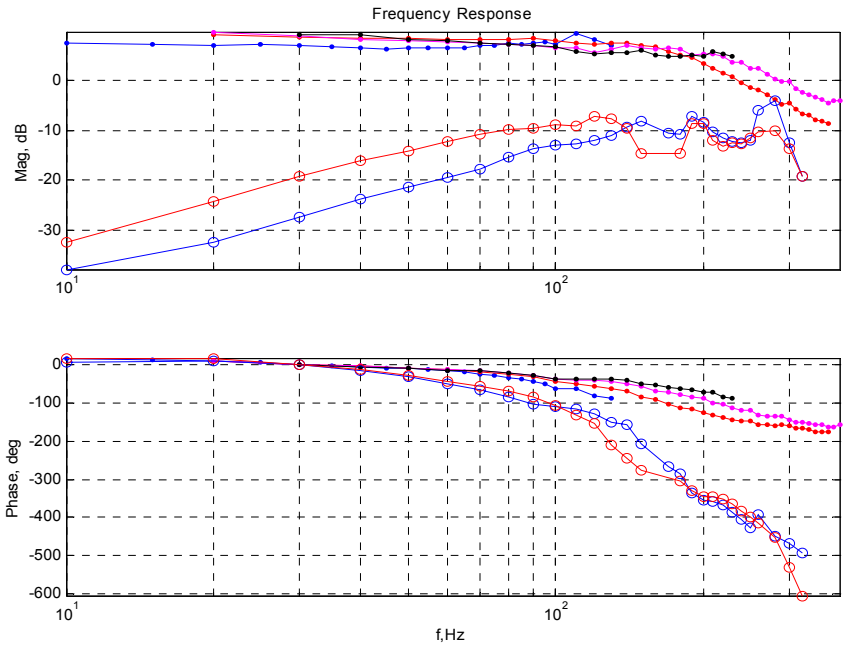


(b) Φ=0.65

**Figure 5.5. OH* Chemiluminescence FRF.** Reaction rate dynamics are similar for the laminar (●) and turbulent (○) flames at low frequencies.

Analogous to the reaction rate dynamics, AFF dynamics of laminar and turbulent flames are similar at low frequencies, as seen in Figure 5.6. The frequency responses begin to diverge at approximately 200 Hz. Here, the phase begins to rise in the turbulent case, instead of continuing to fall as in the laminar frequency response. The divergence suggests that turbulence effects on flame dynamics are significant at frequencies above 200 Hz. It should be noted that convection effects in the laminar flame dynamics become dominant near 200 Hz, also.

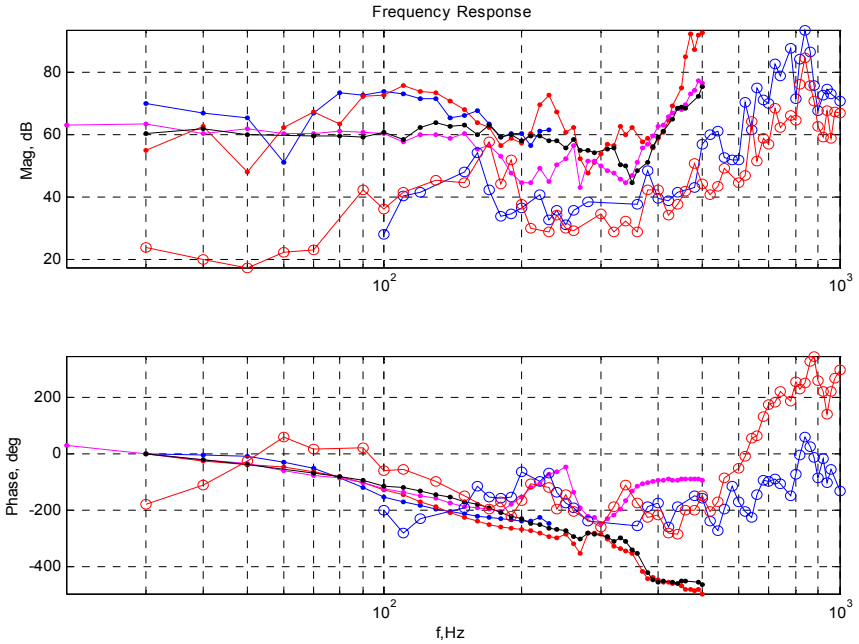


(a) Φ=0.60

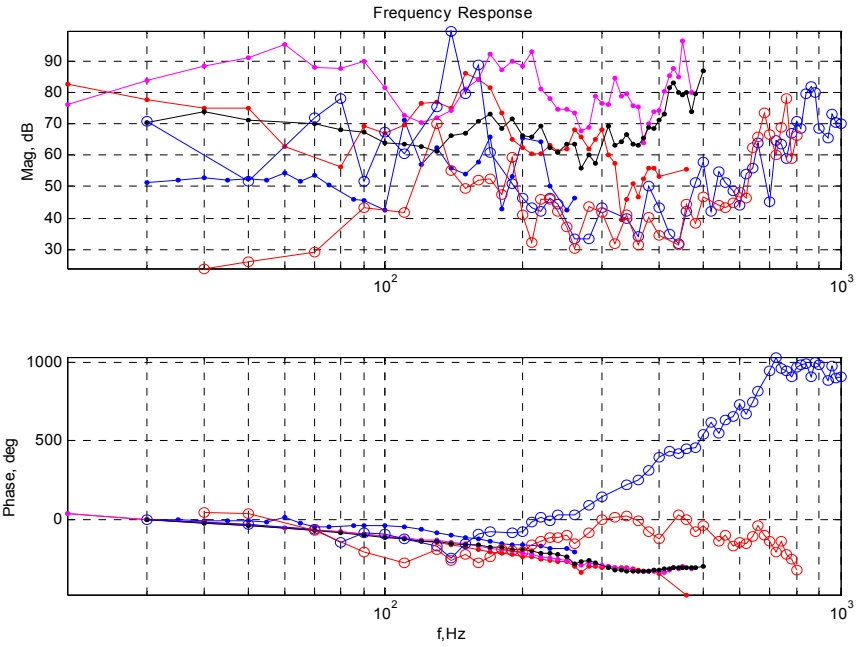


(b) Φ=0.65

**Figure 5.6. Temperature FRF.** AFF dynamics are similar for the laminar (●) and turbulent (○) flames at frequencies below 200 Hz.

**5.3.5 Comparison of Reaction Rate and AFF Dynamics.** The OH* chemiluminescence and temperature frequency responses are shown in Figure 5.7, providing a comparison of reaction rate and AFF dynamics. Magnitudes are scaled to allow comparison. Reaction rate and AFF responses coincide at frequencies below approximately 180 Hz. The first resonance, at ≈ 130 Hz, corresponds for the reaction rate and AFF frequency responses. At frequencies greater that 180 Hz, the frequency responses diverge, indicating thermal diffusion is dominant in this region. This divergence indicates that, at frequencies above 180 Hz, the chemical kinetics no longer provide enough energy to dominate the AFF. The reaction rate and acoustic forcing function dynamics diverge in the same frequency range for laminar flames. Overall, the AFF responses are more lightly damped than the OH* chemiluminescence dynamics. The lightly-damped characteristics may be due to the local measurement of AFF compared to the global measurement of reaction rate. The global measurement would tend to integrate any small, local fluctuations out. Local fluctuations, due to smaller losses, would tend to be lightly damped.

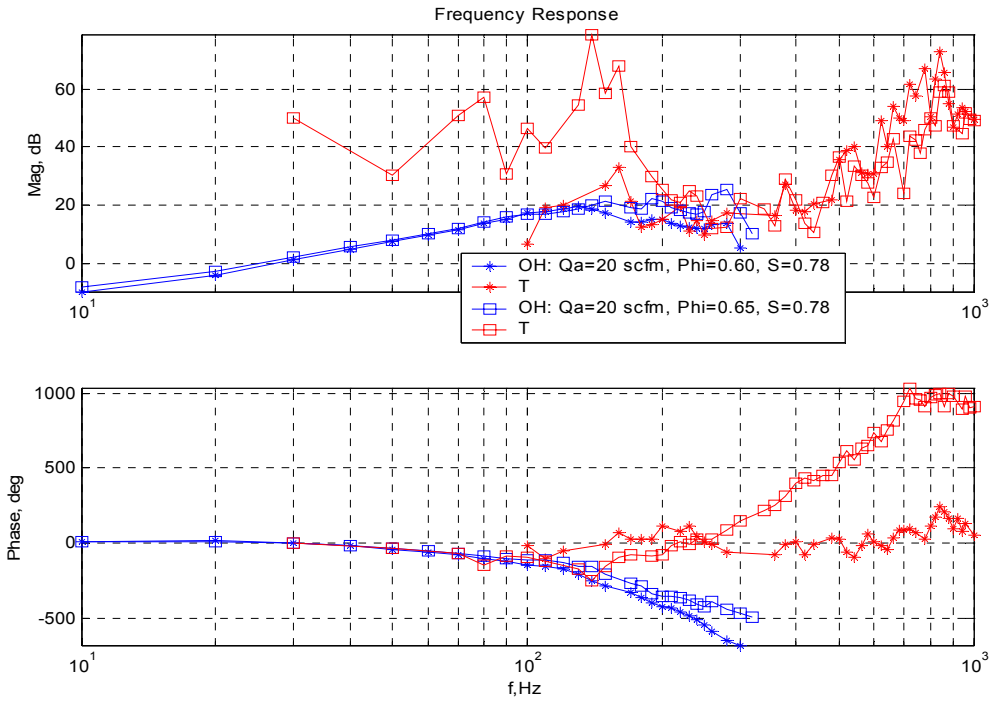


**(a) Qa=20 scfm, S=0.78**

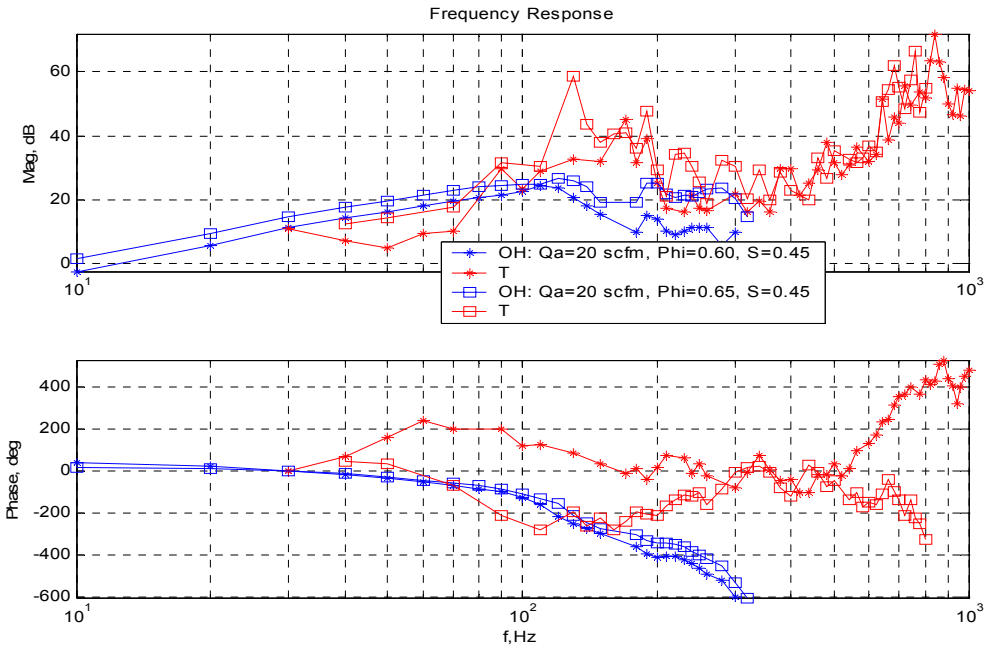


**(b) Qa=20 scfm, S=0.45**

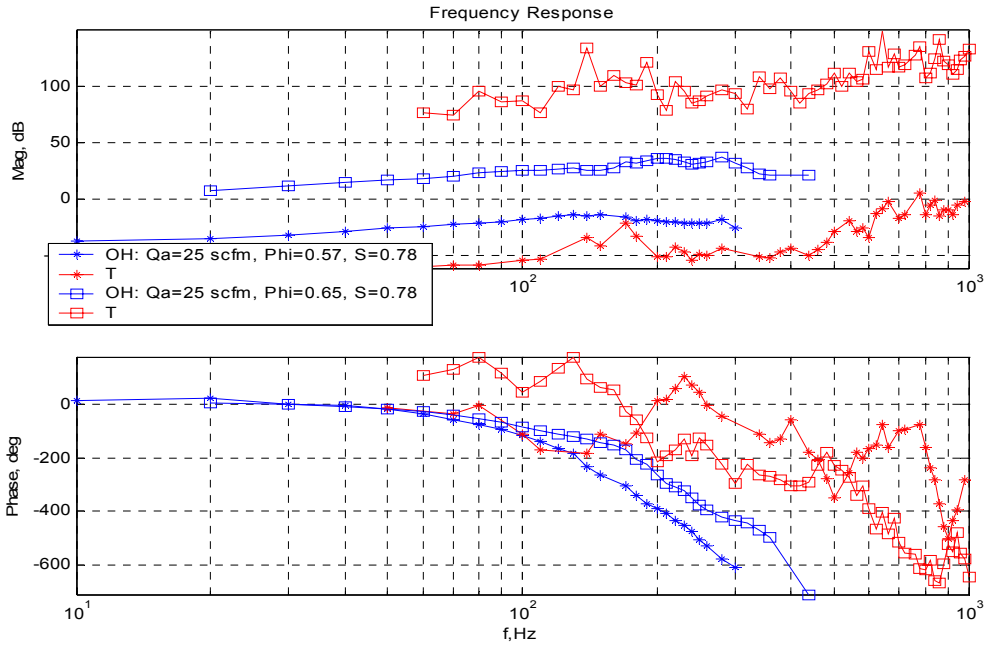


**(c) Qa=25 scfm, S=0.78**

**Figure 5.7. Comparison of OH* Chemiluminescence (OH) and Temperature (T) Frequency Response Functions.** Responses are similar at frequencies below 180 Hz.

## 5.4 Models of Turbulent Flame Dynamics

**5.4.1 Approach.** The approach used to develop models of laminar flame dynamics was also used to formulate models of turbulent flame dynamics. First, an analytical and numerical analysis yields the physical processes that must be measured to capture the acoustic forcing function. It was assumed that the turbulent flame acts as many small laminar flames, or flamelets, so physical and chemical factors in the acoustic forcing function remain the same. Next, measurement techniques are devised to measure the dominant processes, in this case OH* chemiluminescence, product gas temperature, velocity fluctuations, and equivalence ratio fluctuations. Frequency response functions of the OH* chemiluminescence and product gas temperature with respect to velocity fluctuations are then measured. A subsequent study will investigate the frequency response functions with respect to equivalence ratio fluctuations. Dimensionless parameters are determined through dimensional analysis and a literature search. The data is plotted in dimensionless form using these parameters. Finally, low-order dynamic models are fit to the scaled frequency response data.

**5.4.2. Dimensional Analysis.** In addition to the parameters obtained from the dimensional analysis of the laminar conservation equations, several parameters have been shown to be important to turbulent flame dynamics in the literature [3-6]. Swirling flows are characterized by a swirl number, S, the ratio of axial flux of swirl momentum to axial momentum. Gupta [7] gives the swirl number as

$$S = \frac{G_\theta}{G_x (d/2)}$$

$$G_\theta = \int_0^\infty \left(\rho u w + \rho \overline{u' w'}\right) r^2 dr$$

$$G_x = \int \left(\rho u^2 + \overline{\rho u'^2} + (p - p_\infty)\right) r dr$$

$$d/2 = nozzle\ radius$$

For a vane swirler, if 100% efficiency is assumed, the swirl number simplifies to

$$S = \frac{2}{3}\left[\frac{1-(d_h/d)^3}{1-(d_h/d)^2}\right]\tan\phi$$

where $d_h$ is the hub diameter, $d$ is the outer diameter, and $\phi$ is the vane angle. For the 45 degree and 30 degree swirlers used in this study, the swirl numbers are 0.78 and 0.45.

The Damkohler number provides a measure of residence time, or a ratio of the characteristic time of fluid mechanics to chemical kinetics. The Damkohler number is defined as

$$Da = \frac{\tau_{flow}}{\tau_{chemical}} = \frac{(l_o / v'_{rms})}{(\delta_L / S_L)}$$

where $l_o$ is the integral flow length scale (length of the largest flow structure), $v'_{rms}$ is the root-mean-squared magnitude of the turbulent velocity, $\delta_L$ is the laminar flame length, and $S_L$ is the laminar flame speed. The integral flow length was taken as the burner radius. The turbulent velocity was assumed to be 10% of the mean velocity. The laminar flame speed was taken from the correlation

$$S_{L,ref} = -6.67\Phi^3 + 14.29\Phi^2 - 9.48\Phi + 2.15$$

for the adiabatic flame speed [5] and scaled with respect to temperature and pressure using

$$S_L = S_{L,ref}\left(\frac{T}{T_{ref}}\right)^{\gamma}\left(\frac{P}{P_{ref}}\right)^{\beta}$$
$$\gamma = 2.18 - 0.8(\Phi - 1)$$
$$\beta = -0.16 + 0.22(\Phi - 1)$$

The laminar flame length is then

$$\delta_L = \frac{2\alpha}{S_L}$$

where $\alpha$ is the thermal conductivity.

The Karlovitz number is a measure of flame stretch

$$Ka = \frac{\tau_{chem}}{\tau_{Kolomogrov}} = \frac{(\delta_L / S_L)}{(l_k / v'_{rms})}$$

where $l_k$ is the scale of the smallest eddies, or Kolomogrov scale. Flame stretch is the degree to which the deflagration wave is deformed by the fluid mechanics.

Other important parameters include the turbulent Reynold's number and ratio of the Kolomogrov scale to the flame length.

$$\mathrm{Re}_{l_o} = \frac{\rho v'_{rms}\, l_o}{\mu}$$

$$\frac{l_k}{\delta_L} = \frac{l_o\, \mathrm{Re}_{lo}^{-3/4}}{\delta_L}$$

To calculate the Strouhal number, the turbulent flame speed is required. The turbulent flame speed is estimated through the correlation [4]

$$S_T = \left\{ 2 S_L u' \left[ 1 - \frac{S_L}{u'} \left( 1 - e^{-u'/S_L} \right) \right] \right\}^{1/2}$$

$$u' = \left( \frac{1}{\sqrt{3}} \right) \left( \frac{T_{ss}}{T_{ref}} - 1 \right) S_{L,ref}$$

where $T_{ss}$ is the measured steady-state temperature.

Steady-state values of OH* chemiluminescence and temperature were needed to calculate turbulence parameters. The steady-state values, from experiment, are shown in Tables 5.8 and 5.9. The calculated turbulent flame speeds are shown in Figure 5.10. Flame speed increases with equivalence ratio, as expected. Higher swirl creates higher turbulence, and also increases the flame speed. The legend for remaining figures in this chapter is shown in Table 5.11.

**Table 5.8. Steady-State OH* Chemiluminescence.**

| Phi, - | Q=20 scfm, S=0.78 | Q=20 scfm, S=0.45 | Q=25 scfm, S=0.78 |
|---|---|---|---|
| 0.57 | - | - | 0.0035 |
| 0.60 | 0.1089 | 0.0570 | - |
| 0.65 | 0.1248 | 0.1374 | 0.1652 |

**Table 5.9. Steady-State Temperatures.**

| Phi, - | Q=20 scfm, S=0.78 | Q=20 scfm, S=0.45 | Q=25 scfm, S=0.78 |
|---|---|---|---|
| 0.57 | - | - | 1157.45 |
| 0.60 | 1488.55 | 1199.54 | - |
| 0.65 | 1464.64 | 1115.47 | 1402.68 |

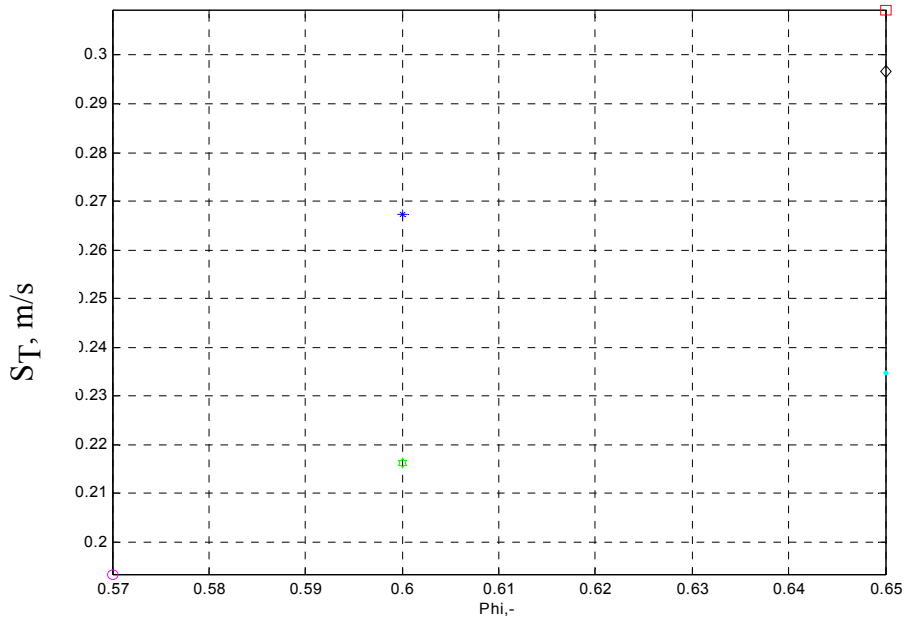


**Figure 5.10. Turbulent Flame Speed.** A correlation was used to calculate the turbulent flame speed.

**Table 5.11. Legend**. The legend applies to the remainder of figures in Chapter 5.

| Symbol | Qa, scfm | Φ | S |
|---|---|---|---|
| * | 20 | 0.60 | 0.78 |
| □ | 20 | 0.65 | 0.78 |
| ○ | 25 | 0.57 | 0.78 |
| ◊ | 25 | 0.65 | 0.78 |
| ○ | 20 | 0.60 | 0.45 |
| ● | 20 | 0.65 | 0.45 |

Premixed, turbulent flames are classically categorized into three regimes, as described in Table 5.12. The Damkohler number is the ratio of the characteristic flow time to the chemical time constant. For this study, the Damkohler numbers are on the

order of $10^4$ to $10^5$, indicating relatively short residence times. The Damkohler numbers are plotted in Figure 5.13. The Damkohler numbers for the conditions studied are grouped closely, indicating they are in the same turbulent combustion regime. The close grouping also helps to explain the similarity of the frequency response data. Aside from the Qa=25 scfm, Phi=0.57 case, the Damkohler number increases with increasing swirl, indicating swirl increases turbulence. The magnitude of the frequency response functions loosely correlates with the inverse of the Damkohler number, suggesting dynamic gain is inversely proportional to the Damkohler number. The Karlovitz number indicates the degree of flame stretch. Karlovitz numbers are on the order of $10^{-4}$ to $10^{-2}$, as seen in Figure 5.15. Thus, the flames are only slightly stretched by the turbulence. These parameters indicate the flame in this study was in the flamelets regime. The flamelets regime in described as many small laminar flames, or flamelets, stabilized in the turbulent flow. Due to the low degree of stretch, the flames retain most characteristics of laminar flames, but are shaped by turbulent structures. The turbulent combustion diagram in Figure 5.14 describes the regimes graphically. The distinction between flame regimes is made somewhat arbitrarily, based on experimental observations. In reality, turbulent flame characteristics are a spectrum ranging from wrinkled laminar flames to well-stirred reactors. A well-stirred reactor is characterized by high turbulence intensities and long residence times. Reactants are perfectly mixed and chemical reactions are assumed to reach steady state.

**Table 5.12. Regimes of Turbulent Premixed Combustion [3].**

| Ka<1 (Da>1) | Ka>1 and Da>1 | Da<<1 |
|---|---|---|
| Flamelets | Thickened Flames | Well-stirred Reactor |
| Flame is thinner than all turbulent scales | Small turbulent scales may enter the flame front | All turbulent time scales are smaller than the chemical time scale |

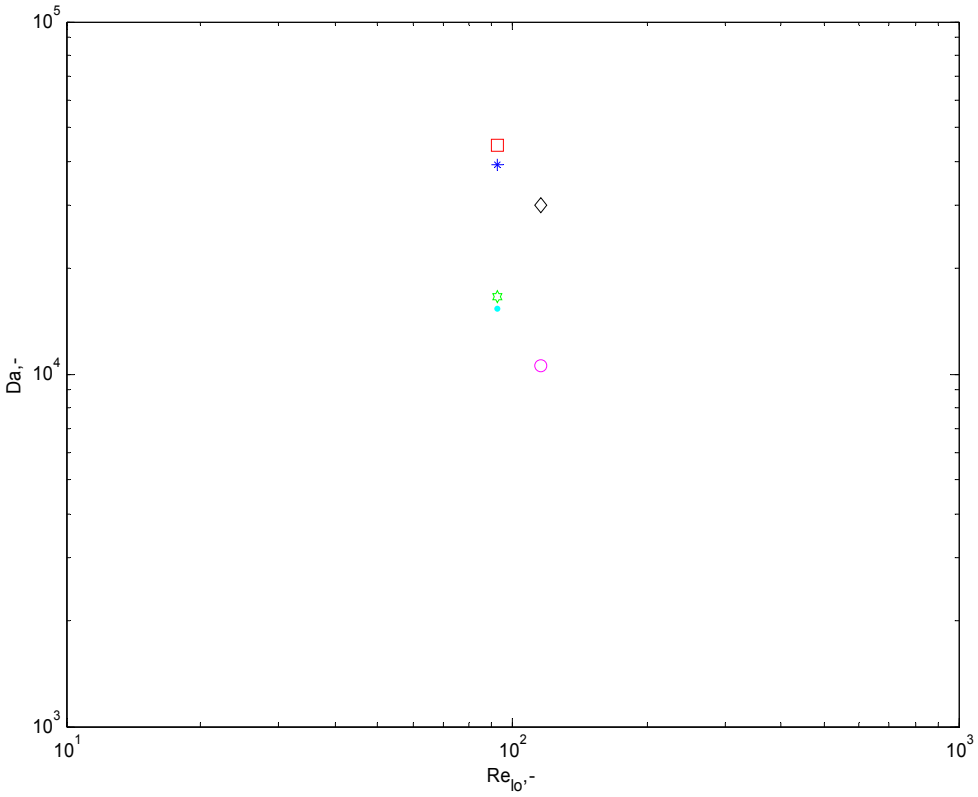


**Figure 5.13. Damkohler Number.** The Damkohler number is inversely proportional to the residence time.

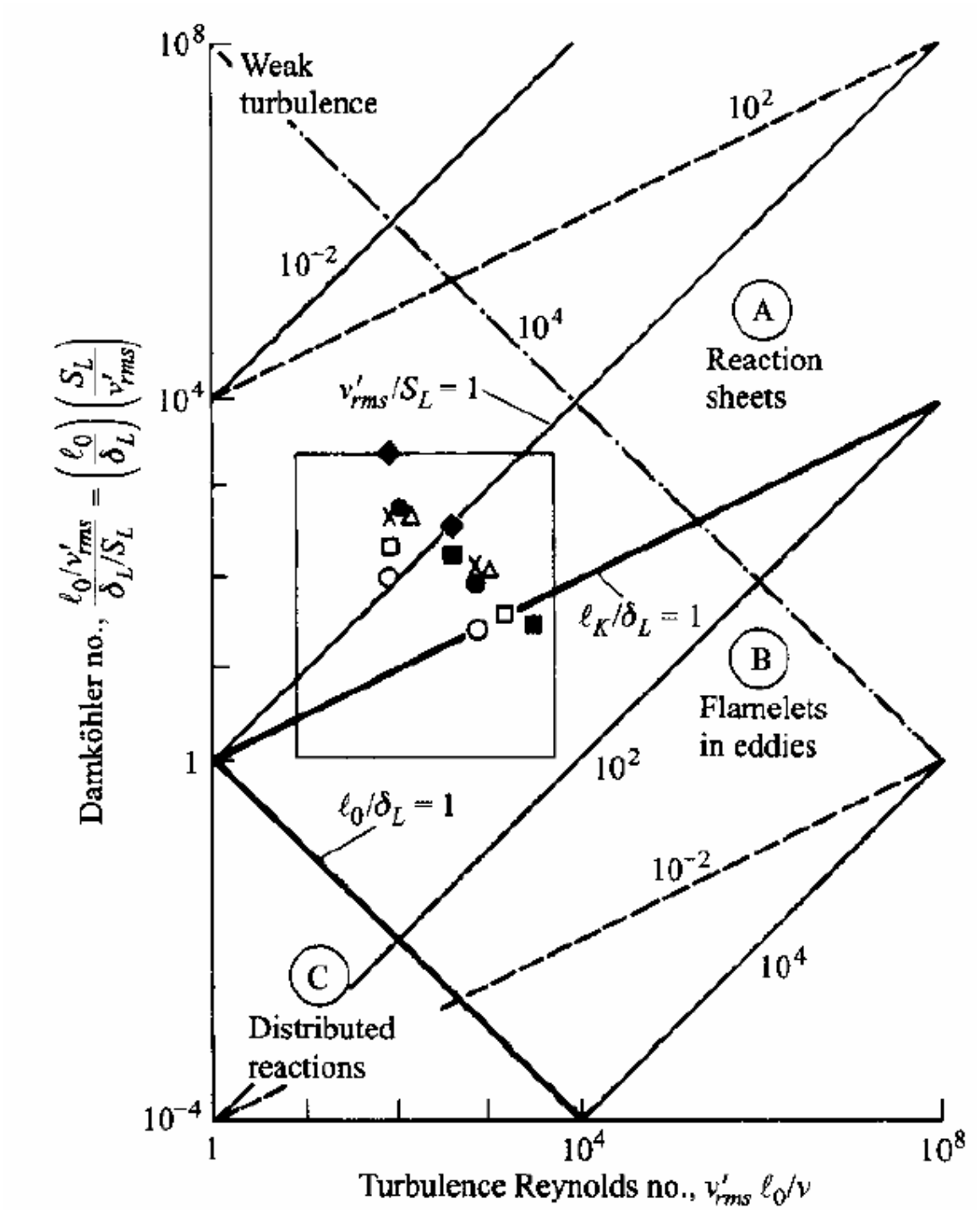


**Figure 5.14. Turbulence Diagram.** Conditions satisfying the Williams-Klimov criterion for the existence of wrinkled flames lie above the solid line $l_o = \delta_L$, and conditions satisfying the Damkohler criterion for distributed reactions fall below the solid line $l_o = \delta_L$. Figure from **[5].**

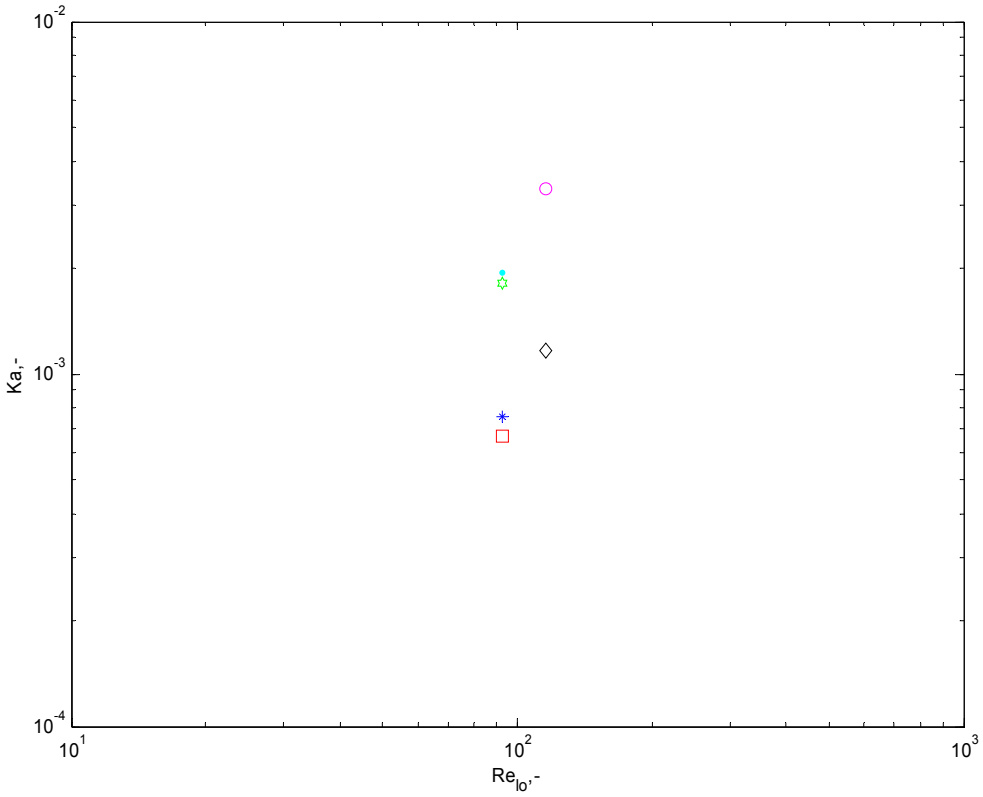


**Figure 5.15. Karlovitz number.** The Karlovitz number indicates the degree of flame stretch.

**5.4.3 Case Models.** Using the parameters from the dimensional analysis, the frequency response functions were plotted in dimensionless form. The OH* chemiluminescence frequency response functions were normalized using

$$M^* = \frac{OH^* / OH^*_{ss}}{u / u_0}$$

where $u_0$ is the turbulent flame speed and the steady-state OH* chemiluminescence values are shown in Table 5.8. The temperature frequency responses were normalized using

$$M^* = \frac{T / T_{ss}}{u / u_0}.$$

The temperature is scaled by the steady state temperature, $T_{ss}$, or the mean of the temperature measured at the beginning and end of each test. The steady-state

temperatures are shown in Table 5.9. The abscissa was normalized using the Strouhal number,

$$St = \frac{l_0}{u_0 t_0} = \frac{\omega R}{u_0}.$$

When plotted in this manner, the data becomes much more compact. For the reaction rate dynamics, transfer functions were fit to the data in the form

$$H_f(j\omega^*) = H_f(s^*) = \frac{Ke^{-s^*\tau}}{\left(s^{*2} + 2\zeta_{p1}\omega_{n,p1}^{*}{}^{2} s^* + \omega_{n,p1}^{*2}\right)\left(s^{*2} + 2\zeta_{p2}\omega_{n,p2}^{*}{}^{2} s^* + \omega_{n,p2}^{*2}\right)\left(s^{*2} + 2\zeta\omega_{n,p3}^{*}{}^{2} s^* + \omega_{n,p3}^{*2}\right)}$$

where $\omega^* = St$, $K$ is the gain, $\tau$ is the time delay, $\zeta$ is the damping ratio, and $\omega_n$ * is the dimensionless resonant frequency. The model parameters are shown in Table 5.14. The pole-zero map is shown in Figure 5.17. Natural frequency is the distance from the origin in the pole-zero map. Damping ratio is the sine of the angle with respect to the real axis. The natural frequency and damping ratio of each resonance is then plotted as a function of equivalence ratio in Figure 5.18. The model parameters remain monotonic with equivalence ratio. The relatively small changes in model parameters indicate that turbulent flame dynamics are similar for flames in the same turbulence regime. The dynamic models of reaction rate dynamics are shown in Figure 5.19. A 6$^{th}$ order system with time delay describes the OH* chemiluminescence frequency responses well.

**Table 5.16. Reaction Rate Model Parameters.**

| Condition | Phi, - | K | Tau | wn,p1* | Z | wn,p2* | Z | wn,p3* | Z |
|---|---|---|---|---|---|---|---|---|---|
| Q=20 scfm, S=0.78 | 0.60 | 8.0E+12 | 1.0E-02 | 170 | 0.35 | 280 | 0.25 | 410 | 0.04 |
| | 0.65 | 8.0E+12 | 5.0E-03 | 190 | 0.35 | 220 | 0.25 | 410 | 0.04 |
| Q=20 scfm, S=0.45 | 0.60 | 2.00E+13 | 5.00E-03 | 210 | 0.1 | 330 | 0.25 | 520 | 0.04 |
| | 0.65 | 2.0E+13 | 5.0E-03 | 210 | 0.10 | 330 | 0.25 | 510 | 0.04 |
| Q=25 scfm, S=0.78 | 0.57 | 5.0E+15 | 8.0E-03 | 300 | 0.15 | 540 | 0.1 | 820 | 0.04 |
| | 0.65 | 5.0E+14 | 1.0E-02 | 280 | 0.10 | 520 | 0.08 | 820 | 0.04 |

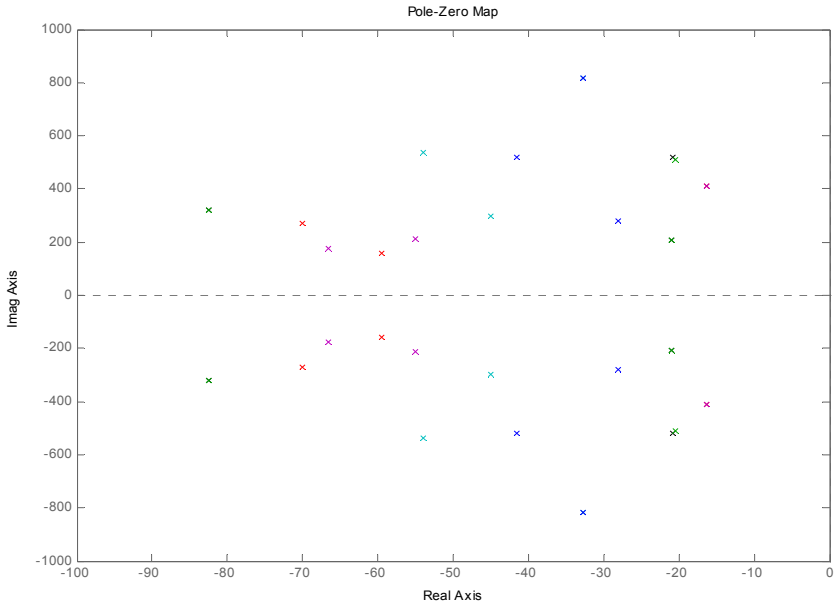


(a)

| Symbol | Qa, scfm | Φ | S |
|---|---|---|---|
| ■ | 20 | 0.60 | 0.78 |
| ■ | 20 | 0.65 | 0.78 |
| ■ | 25 | 0.57 | 0.78 |
| ■ | 25 | 0.65 | 0.78 |
| ■ | 20 | 0.60 | 0.45 |
| ■ | 20 | 0.65 | 0.45 |

(b)

**Figure 5.17. Pole-Zero Map**. X – poles, O - zeros

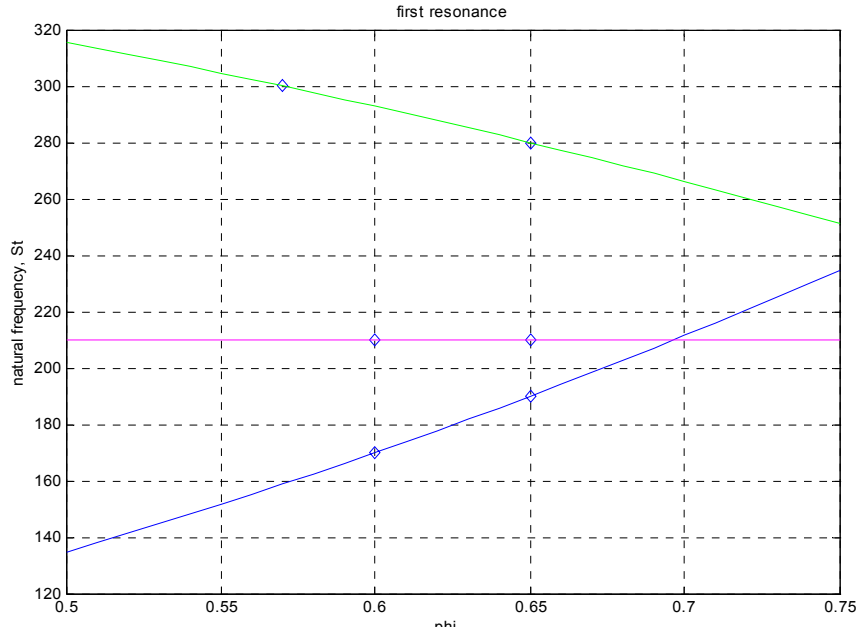


(a) first resonance: natural frequency

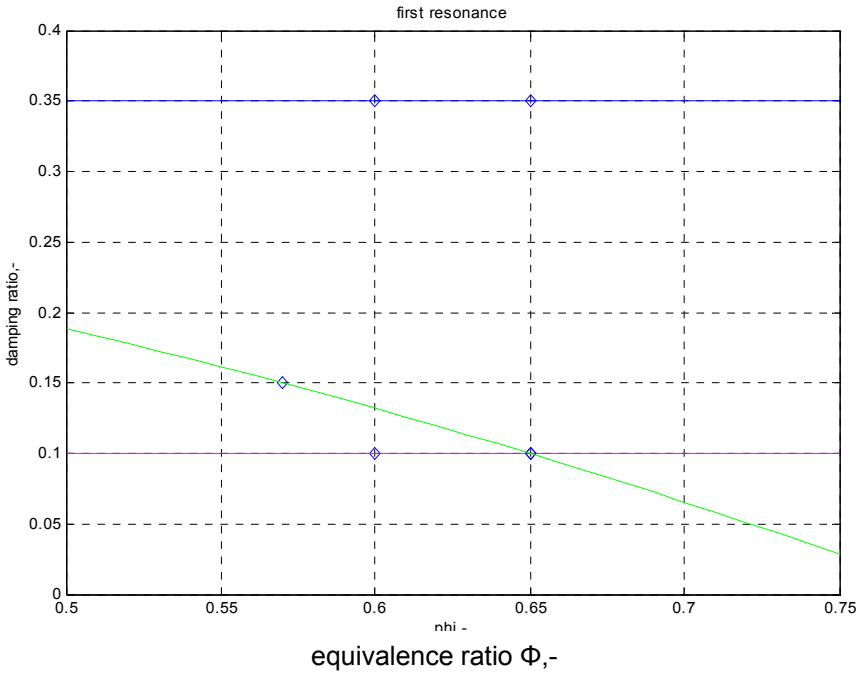


(b) first resonance: damping ratio

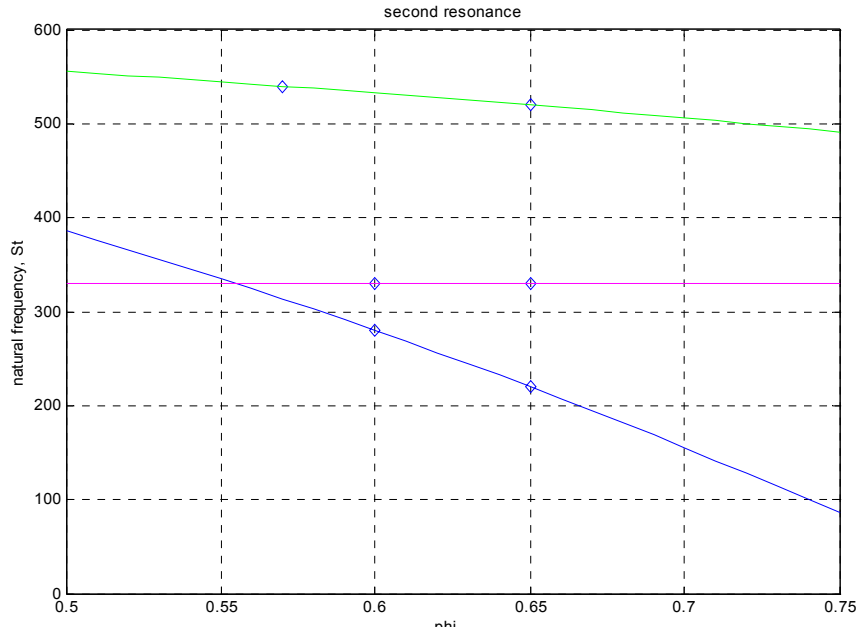


(c) second resonance: natural frequency

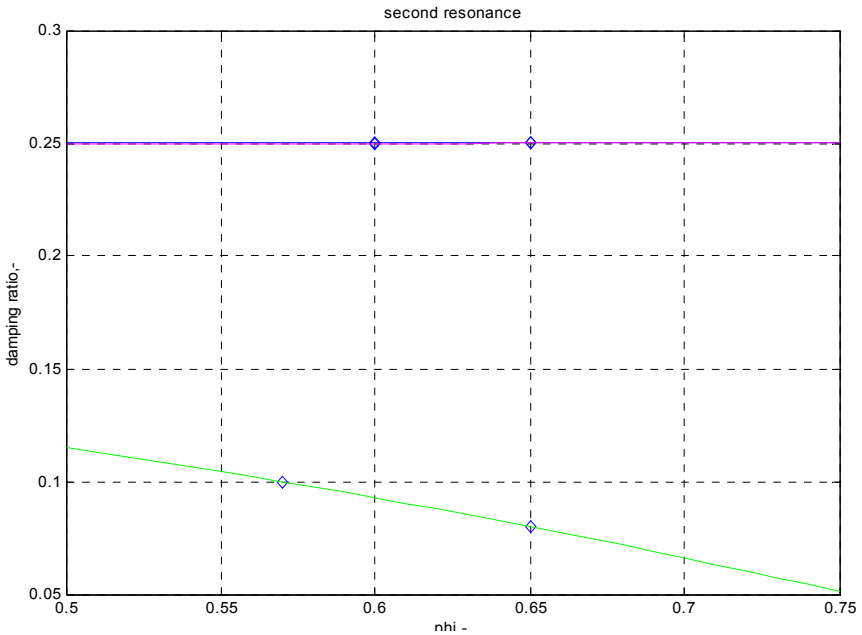


(d) second resonance: damping ratio

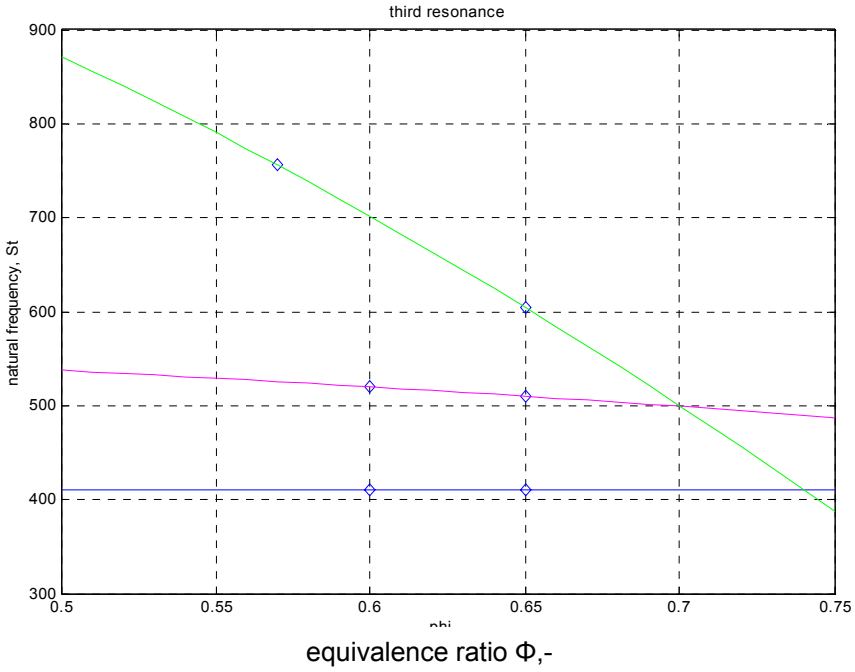


(e) third resonance: natural frequency

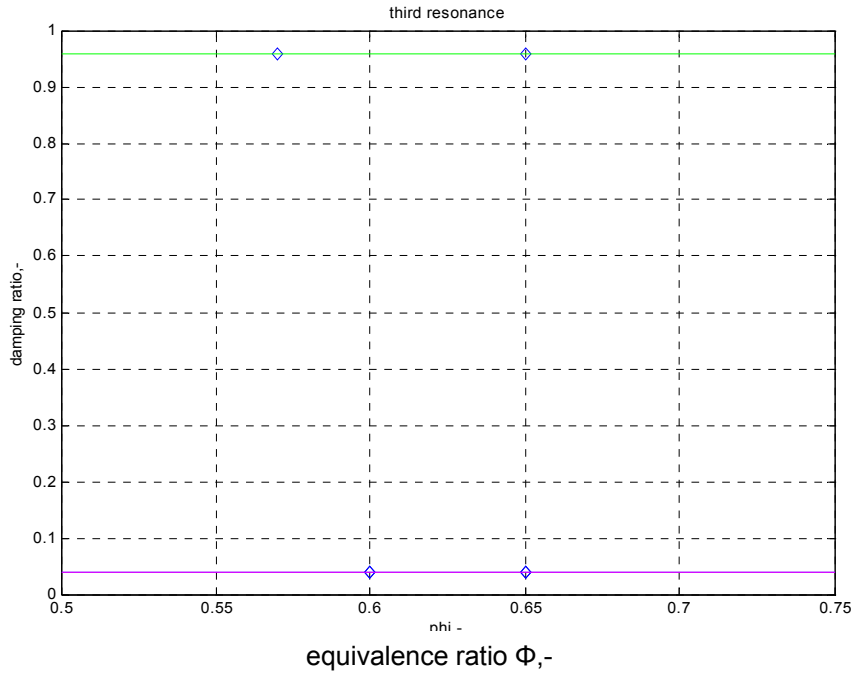


(f) third resonance: damping ratio

**Figure 5.18. Model Parameters.** The parameters are monotonic with equivalence ratio. blue: Q=20, S=0.78, magenta: Q=20, S=0.45, green: Q=25, S=0.78

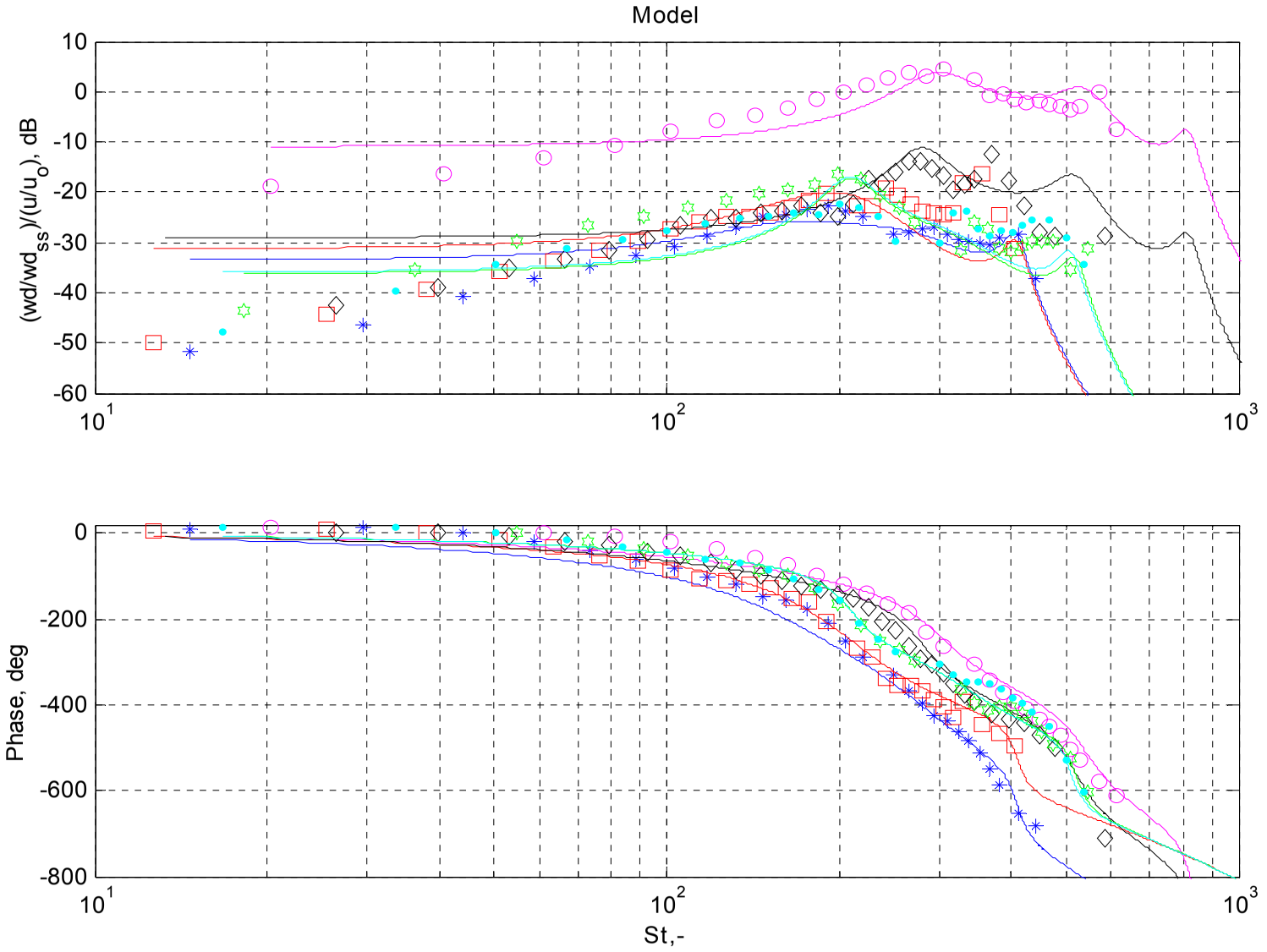
Model
10
0
-10
-20
-30
-40
-50
-60
$10^1$
$10^2$
$10^3$
$(wd/wd_{ss})/(u/u_o)$, dB
0
-200
-400
-600
-800
Phase, deg
St,-

| Symbol | Qa, scfm | Φ | S |
|---|---|---|---|
| * | 20 | 0.60 | 0.78 |
| □ | 20 | 0.65 | 0.78 |
| ○ | 25 | 0.57 | 0.78 |
| ◊ | 25 | 0.65 | 0.78 |
| ○ | 20 | 0.60 | 0.45 |
| ● | 20 | 0.65 | 0.45 |

**Figure 5.19. Reaction Rate Models.** A 6th order system with time delay describes the reaction rate dynamics.

For the acoustic forcing function dynamics, transfer functions were fit to the data in the form

$$H_f(j\omega^*) = H_f(s^*) = \frac{K\left(s^{*2} + 2\zeta_{z1}\omega^*_{n,z1}{}^2 s^* + \omega^{*2}_{n,p1}\right)\left(s^{*2} + 2\zeta_{z2}\omega^*_{n,z2}{}^2 s^* + \omega^{*2}_{n,z2}\right)}{\left(s^{*2} + 2\zeta_{p1}\omega^*_{n,p1}{}^2 s^* + \omega^{*2}_{n,p1}\right)\left(s^{*2} + 2\zeta_{p2}\omega^*_{n,p2}{}^2 s^* + \omega^{*2}_{n,p2}\right)}$$

where $\omega^* = St$, $K$ is the gain, $\zeta$ is the damping ratio, and $\omega_n{}^*$ is the dimensionless resonant frequency. The model parameters are shown in Table 5.20. The pole-zero map is shown in Figure 5.21. The natural frequency and damping ratio of each resonance is then plotted as a function of equivalence ratio in Figure 5.22. The model parameters remain are monotonic with equivalence ratio. The relatively small changes in model parameters indicate that turbulent flame dynamics are similar for flames in the same turbulence regime. The dynamic models of reaction rate dynamics are shown in Figure 5.23. A 4th order system describes the AFF frequency responses well, as there are four roots in the characteristic equation.

**Table 5.20. AFF Model Parameters.** The turbulent AFF is modeled with a 4th order system.

| Condition | Phi, - | K | wn,z1* | Z | wn,z2* | Z | wn,p1* | Z | wn,p2* | Z |
|---|---|---|---|---|---|---|---|---|---|---|
| Q=20 scfm, S=0.78 | 0.60 | 2.0E-02 | 290 | 0.20 | 420 | 0.2 | 230 | 0.08 | 1200 | 0.03 |
| | 0.65 | 2.0E-02 | 280 | 0.20 | 520 | 0.2 | 170 | 0.05 | 1100 | 0.03 |
| Q=20 scfm, S=0.45 | 0.60 | 4.0E-03 | 400 | 0.30 | 800 | 0.2 | 300 | 0.08 | 1500 | 0.03 |
| | 0.65 | 6.0E-03 | 320 | 0.20 | 620 | 0.2 | 280 | 0.05 | 1200 | 0.03 |
| Q=25 scfm, S=0.78 | 0.57 | 1.0E-02 | 450 | 0.20 | 700 | 0.2 | 350 | 0.05 | 1300 | 0.03 |
| | 0.65 | 2.0E-02 | 300 | 0.20 | 520 | 0.2 | 200 | 0.08 | 1100 | 0.03 |

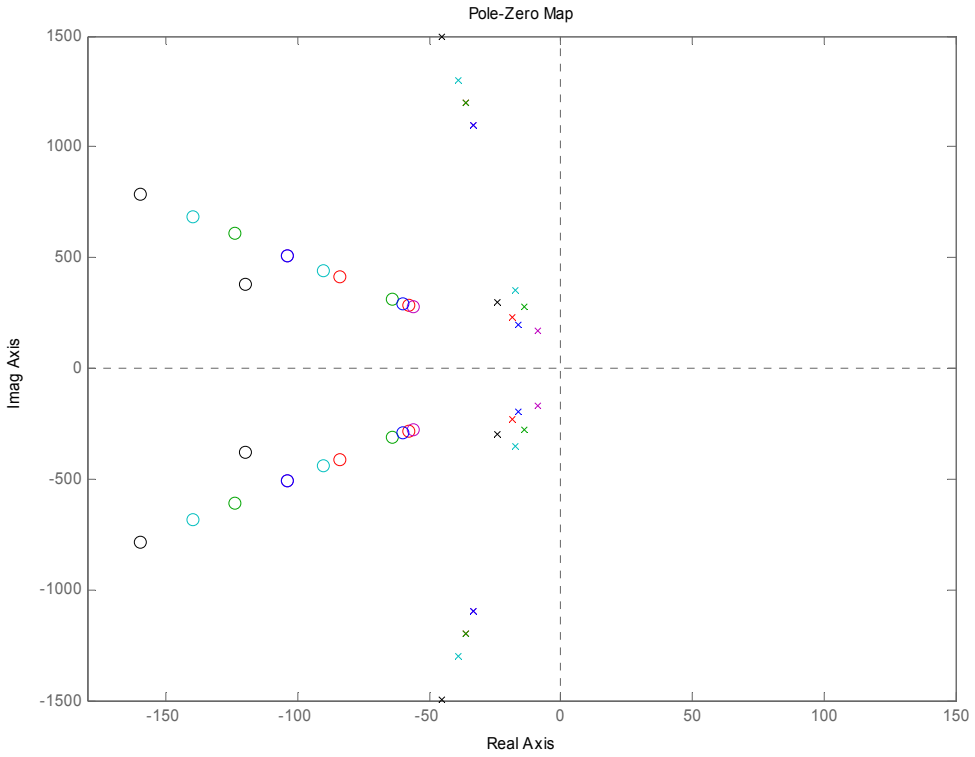


(a)

| Symbol | Qa, scfm | Φ | S |
|---|---|---|---|
| ■ | 20 | 0.60 | 0.78 |
| ■ | 20 | 0.65 | 0.78 |
| ■ | 25 | 0.57 | 0.78 |
| ■ | 25 | 0.65 | 0.78 |
| ■ | 20 | 0.60 | 0.45 |
| ■ | 20 | 0.65 | 0.45 |

(b)

**Figure 5.21. Pole-Zero Map**. X – poles, O - zeros

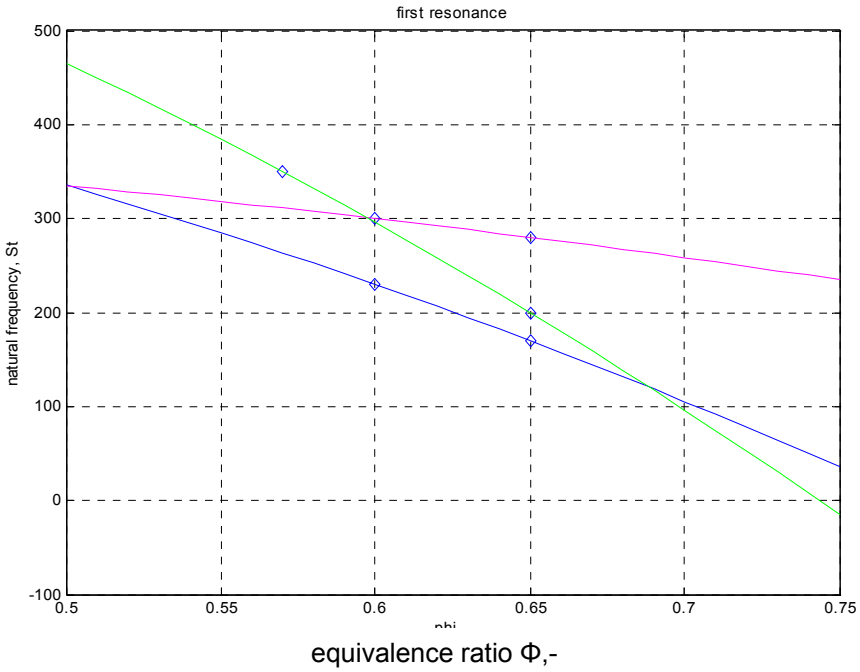


(a) first resonance: natural frequency

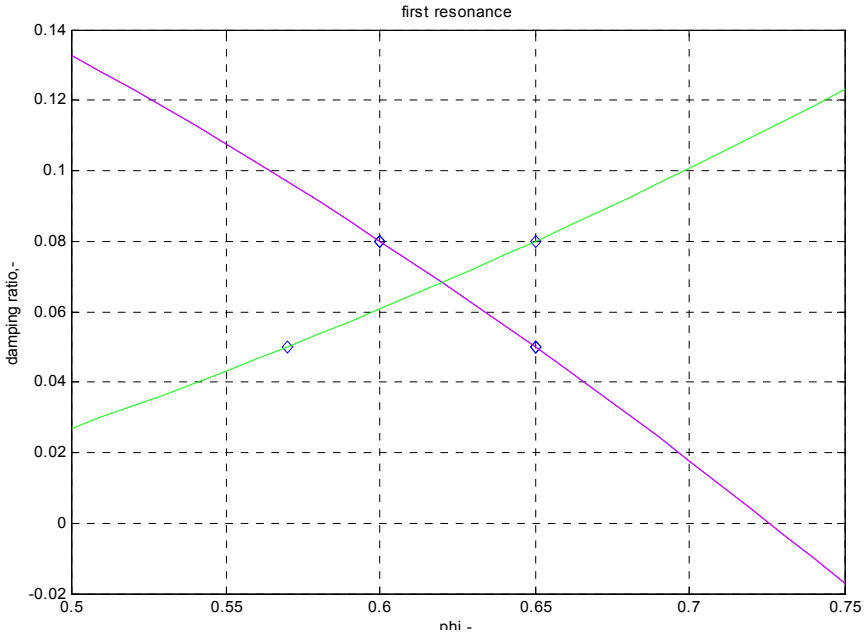


(b) first resonance: damping ratio

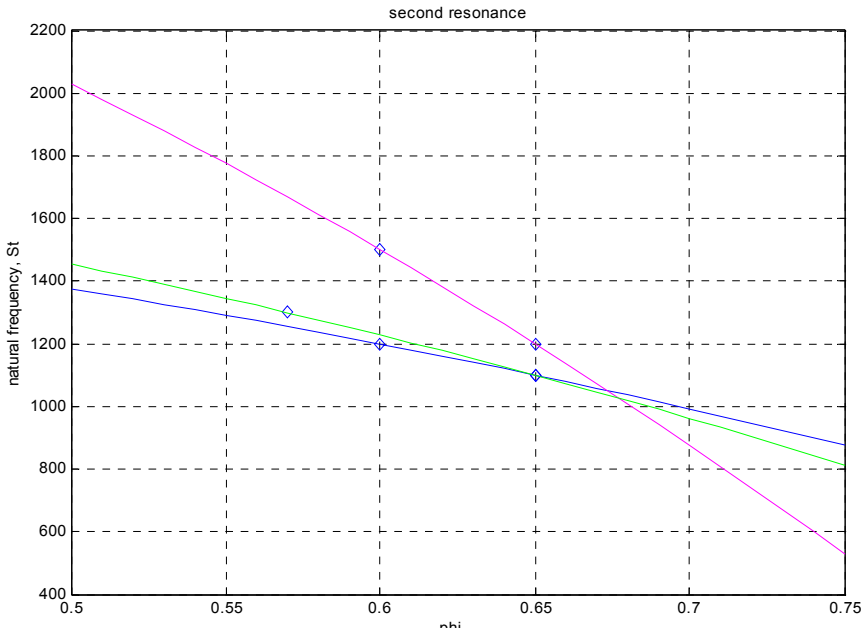


(c) second resonance, natural frequency

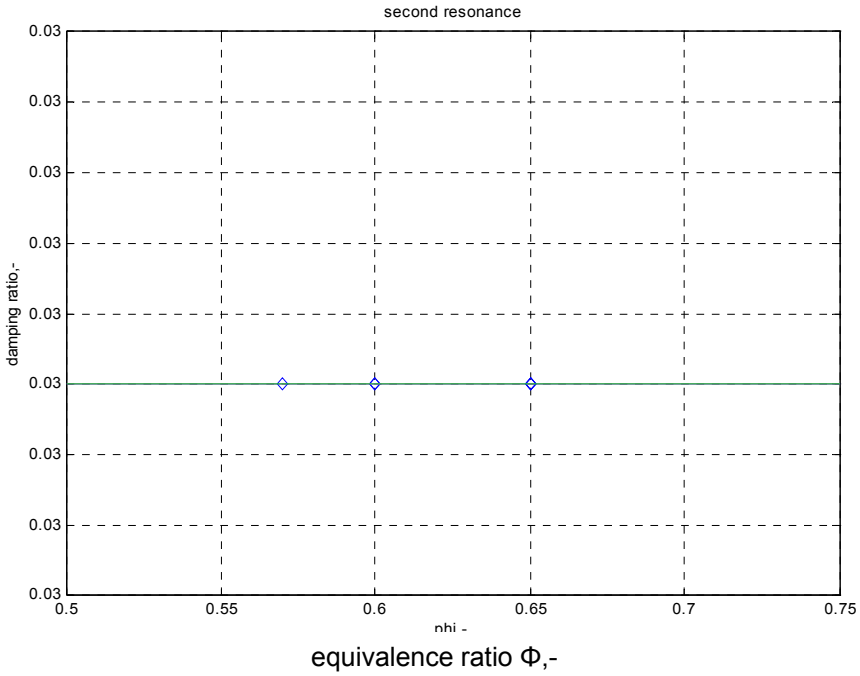


(d) second resonance: damping ratio

**Figure 5.22. Model Parameters**. The parameters vary with equivalence ratio. blue: Q=20, S=0.78, magenta: Q=20, S=0.45, green: Q=25, S=0.78

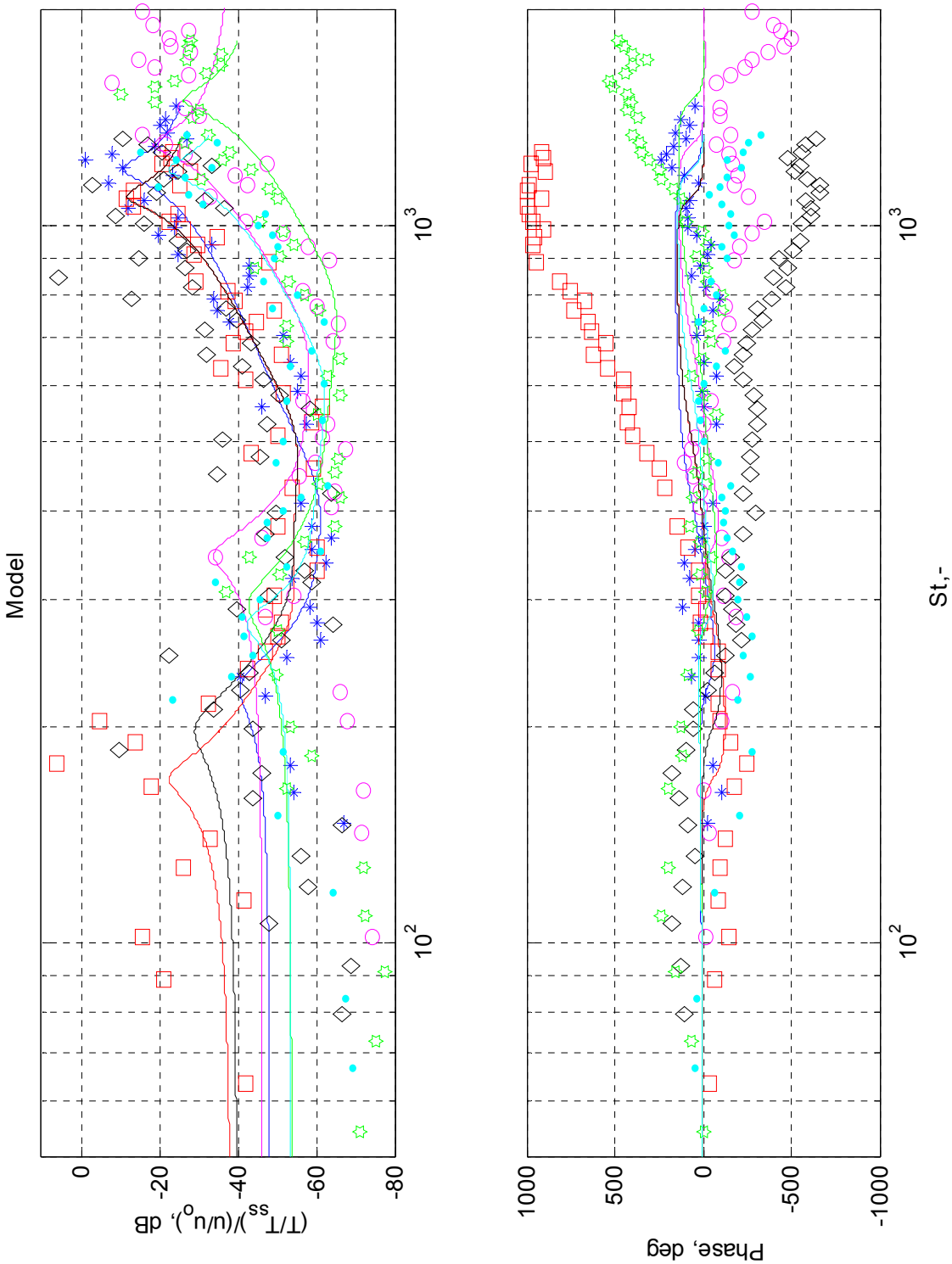
Model
(T/T_ss)/(u/u_o), dB
0
-20
-40
-60
-80
10^2
10^3
Phase, deg
1000
500
0
-500
-1000
St,-

| Symbol | Qa, scfm | Φ | S |
|---|---|---|---|
| * | 20 | 0.60 | 0.78 |
| □ | 20 | 0.65 | 0.78 |
| ○ | 25 | 0.57 | 0.78 |
| ◊ | 25 | 0.65 | 0.78 |
| ○ | 20 | 0.60 | 0.45 |
| ● | 20 | 0.65 | 0.45 |

**Figure 5.23. Acoustic Forcing Function Models.** The acoustic forcing function was modeled with 4 zeros and 4 poles.

**5.4.4 General Model**. As all of the frequency responses exhibit similar characteristics, a model was developed that describes the majority of the data well. The model is in the same form as the case model for the acoustic forcing function. The parameters for the general model are shown in Table 5.24. The model is plotted against the data in Figure 5.25. The Qa=20 scfm, Φ=0.65, S=0.78 case diverges the most from the model. This case also exhibits the highest Damkohler number (and lowest Karlovitz number). Thus, the general model may only be valid for a range of flows, as turbulent flame dynamics are dependent on the Damkohler and Karlovitz numbers. The general model could be applied when a single model is needed to describe turbulent flame dynamics, such as in control algorithms.

**Table 5.24. General Model Parameters.** The general model describes a large portion of the data well.

| K | wn,z1* | Z | wn,z2* | Z | wn,p1* | Z | wn,p2* | Z |
|---|---|---|---|---|---|---|---|---|
| 2.0E-02 | 350 | 0.30 | 600 | 0.2 | 250 | 0.08 | 1150 | 0.03 |

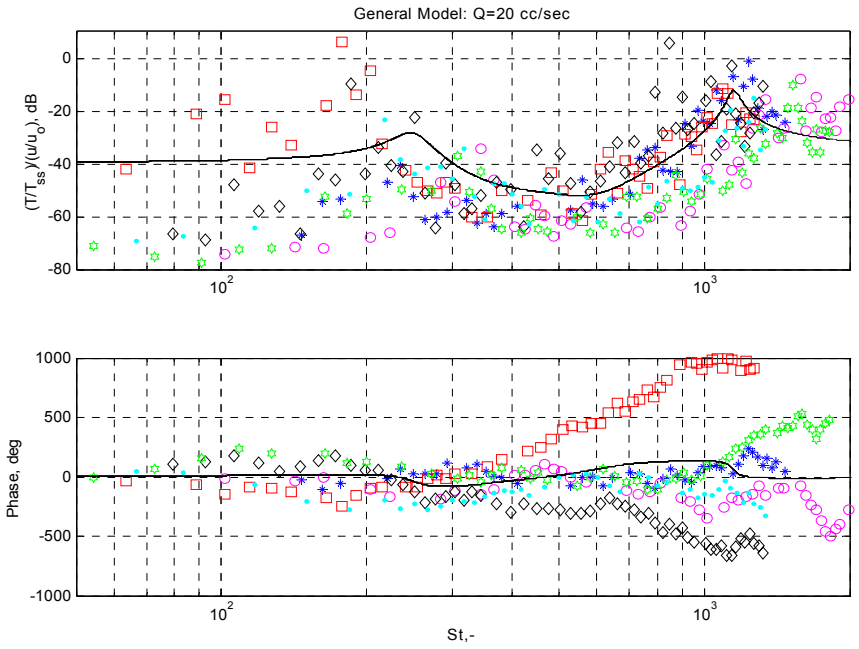


| Symbol | Qa, scfm | Φ | S |
|---|---|---|---|
| * | 20 | 0.60 | 0.78 |
| □ | 20 | 0.65 | 0.78 |
| ○ | 25 | 0.57 | 0.78 |
| ◊ | 25 | 0.65 | 0.78 |
| ○ | 20 | 0.60 | 0.45 |
| ● | 20 | 0.65 | 0.45 |

**Figure 5.25. General Model.** The general model describes the majority of the cases.

## 5.5 Summary and Conclusions

The dynamics of turbulent premixed flames were investigated to determine the effect of turbulence on flame dynamics. OH* chemiluminescence was used as an indicator of heat release rate. Product gas temperature, measured via water absorption, was used as an indicator of the acoustic forcing function. A range of flow rates, equivalence ratios, and swirl numbers were investigated.

Turbulent, swirl-stabilized flames are used in many current gas turbines for power generation. Turbulent combustors are also employed in engines and augmentors for

aerospace applications. The simple models of turbulent flame dynamics developed in this study elucidate the dominant characteristics of turbulent premixed flames. The models can be used to predict and control thermoacoustic instabilities.

Laminar and turbulent flame dynamics are found to be similar at low frequencies. At frequencies above ≈200 Hz, the frequency responses diverge, attributed to the influence of turbulence. Reaction rate dynamics of turbulent flames exhibit two high-frequency resonances not observed in laminar flames. Accordingly, the turbulent reaction rate dynamics are modeled with a $6^{th}$ order system, while the laminar reaction rate dynamics required a $2^{nd}$ order system. The acoustic forcing function dynamics of turbulent flames also exhibited a strong, high-frequency resonance not seen in the laminar flames. The turbulent AFF dynamics also showed evidence of zeros, resulting in $4^{th}$ order models compared to the $2^{nd}$ order models used for the laminar AFF dynamics.

Analogous to the laminar flame dynamics, the reaction rate and AFF frequency responses are similar for low frequencies. The agreement suggests that chemical heat release dominates the acoustic forcing function in this range. At higher frequencies, the reaction rate and AFF diverge; signifying thermal diffusion dominates the acoustic forcing function at high frequencies. Physically, the dominance of heat transfer effects means that the flame, or combustion zone, is acting as a DC (steady) heat source, much in the same way as the honeycomb acts as a DC heat source in the laminar burner. The unsteady flow, caused by acoustics, through the DC heat source causes an unsteady temperature. Flame movements caused by an unsteady flow field would also result in an unsteady temperature field in time. This conclusion is counter-intuitive, as one would assume that reaction rate dominates turbulent flame dynamics as there is no flame holder. This may also provide insight into why high-frequency instabilities are often not predicted by conventional means. In the gas turbine and propulsion industry, thermoacoustic instabilities are often observed at frequencies in the 1-10kHz range. Fluid mechanical effects on the acoustic forcing function, such as unsteady heat transfer due to unsteady velocities or coherent fluid structures, have the ability to respond at these high frequencies.

Although only the flamelet regime of turbulent premixed flames was investigated, the insight into the dominant factors affecting turbulent flame dynamics can provide

intuition for all turbulent flame dynamics. The low-order models developed in this study can be used to predict thermoacoustic instabilities, and develop control algorithms, for turbulent flames in the flamelet regime. The models can also be used as an estimate of turbulent premixed flame dynamics in general. Most importantly, the knowledge gained on the ranges where chemical and heat transfer effects are dominant can be used to further the understanding of flame dynamics.

## Bibliography


1. Haber, L., *The relationship between OH chemiluminescence and chemical reaction rate in laminar premixed combustion*, in *Mechanical Engineering*. 2000, Virginia Tech: Blacksburg, VA.
2. Khanna, V., *A study of the dynamics of laminar and turbulent fully and partially premixed flames*, in *Mechanical Engineering*. 2001, Virginia Tech: Blacksburg, VA.
3. Poinsot, T. and D. Veynante, *Theoretical and Numerical Combustion*. 2001.
4. Lewis, B. and G. Elbe, *Combustion, Flames and Explosions of Gases*. 3 ed. 1987: Academic Press.
5. Turns, S., *An introduction to combustion*. 2 ed. 1999: McGraw-Hill Science/Engineering/Math.
6. Williams, F.A., *Combustion Theory*. 2 ed. 1985: The Benjamin/Cummings Publishing Co., Inc.
7. Gupta, A.K., D.G. Lilley, and N. Syred, *Swirl Flows*. 1984, London, England: Abacus Press, Inc.